J Mater Sci: Mater Med (2009) 20:203–214
DOI 10.1007/s10856-008-3539-6

The use of dual beam ESEM FIB to reveal the internal ultrastructure of hydroxyapatite nanoparticle-sugar-glass composites

David M. Wright · John J. Rickard · Nigel H. Kyle · Tevor G. Gard · Harald Dobberstein · Michael Motskin · Athene M. Donald · Jeremy N. Skepper

Received: 25 March 2008 / Accepted: 10 July 2008 / Published online: 20 August 2008

Abstract Microparticles (MP) spray dried from hydroxyapatite (HA) nanoparticle (NP) sugar suspensions are currently under development as a prolonged release vaccine vehicle. Those with a significant sugar component cannot be sectioned by ultramicrotomy as resins are excluded by the sugar. Focused ion beam (FIB) milling is the only method to prepare thin sections that enables the inspection of the MPs ultrastructure by transmission electron microscopy (TEM). Several methods have been explored and we have found it is simplest to encapsulate MPs in silver dag, sandwiched between gold foils for FIB-milling to enable multiple MPs to be sectioned simultaneously. Spray dried MPs containing 80% sugar have an inter-nanoparticle separation that is comparable with NP size (~50 nm). MPs spray dried with 50% sugar or no sugar are more tightly packed. Nanoporosity in the order of 10 nm exists between NPs. MPs spray dried in the absence of sugar and sectioned by ultramicrotomy or by FIB-milling have comparable nanoscale morphologies. Selected area electron diffraction (SAED) demonstrates that the HA remains (substantially) crystalline following FIB-milling.

D. M. Wright (✉) · M. Motskin · J. N. Skepper
Multi-Imaging Centre, Department of Physiology, Development and Neuroscience, School of Biological Sciences, University of Cambridge, Anatomy Building, Downing Street, Cambridge CB2 3DY, UK
e-mail: dmw31@cam.ac.uk

J. J. Rickard · H. Dobberstein · A. M. Donald
Department of Physics, Cavendish Laboratory, University of Cambridge, J J Thomson Avenue, Cambridge CB3 0HE, UK

N. H. Kyle · T. G. Gard
Cambridge Biostability Ltd., Unit 184, Cambridge Science Park, Milton Road, Cambridge, Cambridgeshire CB4 0GA, UK

1 Introduction

Sugar-glass hydroxyapatite, nanoparticle composite microparticles are currently under evaluation as a sustained delivery system for vaccines. The sugar glass phase stabilises protein antigens for storage, without refrigeration, in a non-aqueous delivery fluid. The NP component was originally added to make the MPs neutrally buoyant in the carrier liquid but it has become evident they also prolong antigen release. The arrangement of the NPs within the vitreous sugar-glass matrix of the MP will provide information underlying the mechanism of prolonged vaccine release observed in vivo. MPs consist of thousands of lozenge shaped, single crystal HA NPs, approximately 14 nm wide and 60 nm long, vitrified in a sugar-glass or amino-glass matrix. These spray dried (SD) micro-particles range from 100 nm to 5 μm in diameter. Their internal organisation cannot be studied as bulk particles using transmission electron microscopy (TEM) because they are too thick.

Ultramicrotomy is an established method of obtaining suitably thin (<100 nm), sections of hydroxyapatite composite materials such as fully mineralised bone [1, 2]. Though, routinely used for sectioning soft tissues, harder materials including sintered HA [3], semiconductor films [4], ZnO [5], BN and even diamond itself [6] can be sectioned using a diamond knife with an appropriate edge profile. The use of knives with wedge angles of 35° or less is preferred for very hard materials. The mechanical stresses imposed when cutting hard materials, with knives with a wedge angle of 45° that are commonly used for softer materials readily introduces flaws and artefacts into sections of dense materials [5].

Focused Ion beam (FIB) milling avoids the generation of mechanical artefacts when thinning sections for viewing

in the TEM as it uses energetic ions to ablate material at a very localised (<5 nm) level, instead of cutting mechanically. It is usually undertaken in an instrument that combines a conventional scanning electron microscope (SEM) column for viewing the milling process and a scanning ion beam that not only mills but also generates an image from the secondary electrons produced when the ions interact with the sample material [7]. Preparing thin sections or foils by the FIB techniques is often regarded as much more site specific than ultramicrotomy because the region that is being thinned can be directly observed, at high resolution, during sectioning [8]. This site specific capability gives FIB milling a major advantage over broad ion beam (BIB) milling or electropolishing that are often used on harder inorganic materials [9].

FIB milling was initially developed to study the ultrastructure of semiconductor materials [10] although, it is increasingly being applied to a diverse range of materials including biological [11, 12] and biomaterial specimens. It is especially useful when characterising the interface between materials of differing mechanical moduli. In this case ultramicrotomy is difficult due to the extreme heterogeneity between the differing densities of the phases being sectioned. FIB-milling has already been used to prepare thin foils of the interface between bone and ceramic [13] and cells and ceramic [14], mineral [15] or metal [16]. The study of fractures at the submicrometre level has been transformed by the development of focused ion beam techniques [17] that facilitates the imaging of submicrometre sized inclusions within diamond [18]. TEM specimens of apatite–protein composites such as human tooth enamel [19] human dentine [20] and synthetically produced fluorapatite–gelatine composite particles [21] have been prepared by FIB milling. Cryo-FIB techniques, that avoid the generation of mechanical artefacts and the need for chemical fixation [22] can be used to make thin foils, similar to those produced by cryo-ultramicrotomy. They have recently been used to prepare thin sections of hydrated Escherichia coli [23] and mammalian cells [24].

The affinity of proteins as well as other organic molecules for calcium phosphates is well established. This affinity for HA has enabled the separation of a large range of proteins [25, 26] by column chromatography. Resorbable, calcium phosphate ceramics have been developed as delivery vehicles because of their affinity for growth factors [27, 28], antibiotics [29, 30], anticancer drugs [31–33] and enzymes [34]. These carriers can be incorporated into commercial bone cements [35] and bone replacements. MPs spray dried solely from HA precipitates [36] have already been incorporated into hard tissue replacement materials as slow release drug carriers. The rate of antigen release from these systems will be influenced by the physico–chemical interaction between HA and the protein as well as the dissolution rate of the HA NPs in the in vivo milieu. Importantly, both of these factors can be manipulated by altering the chemistry of the NPs to vary release rates. Entrapment of the antigen inside the mesoporous MP may also be an important mechanism controlling the rate of antigen release from the MP. Antigen release rate will vary in a complex manner dependant on both MP porosity and HA chemistry as is the case for release of growth factors from bone graft material [37]. MP porosity is dependent on the amount of space between the NPs and is a function of NP packing density and arrangement inside the spray dried particles. Spray drying with various concentrations of trehalose is expected to influence this internal morphology. This can potentially vary the rate of antigen release by modifying the nano-porosity of the MP as well as the amount of NP bound antigen present in the MP.

Techniques for imaging the nanoporosity of MPs with varying sugar content are essential. Those with a significant sugar component cannot be infiltrated with resin. Methods of sectioning particles without mechanical stabilisation with resin are essential. The purpose of this study was to investigate the use of FIB-milling techniques for sectioning MPs in the presence and absence of sugar and to make comparison with sections prepared by ultramicrotomy.

2 Materials and methods

2.1 Materials

HA NP were prepared, after the method of Kumta et al. [38], by adding 2 l of 150 mM calcium chloride ($CaCl_2 \cdot 2H_2O$, Sigma-Aldrich) to 2 l 100 mM trisodium orthophosphate dodecahydrate ($Na_3PO_4 \cdot 12H_2O$, Sigma-Aldrich) and stirring thoroughly in an ultrasonic bath (FS200, Decon, UK) for 1 h at ambient temperature. NP suspensions were then washed thoroughly in deionised water and sterilised by autoclaving at 121°C for 15 min in an autoclave (Vario 19, Dixons, UK). After washing and sterilization the concentration was adjusted to 30 mg/ml.

To produce MP without sugar, this suspension was used directly as the feedstock to the spray dryer. Trehalose was added to the NP suspension at a ratio of 50:50 w/w and the concentration adjusted to 30 mg/ml (total solids added) as the feedstock for producing MP with 50% sugar. Trehalose was added to the NP suspension at a ratio of 20:80 w/w NP:trehalose and the concentration adjusted to 30 mg/ml as the feedstock for producing MP with 80% sugar.

The feedstock was maintained in moderate agitation by a magnetic stirrer (Ikamag, USA) and fed into the spray dryer using the built-in peristaltic pump with a feed flow

rate of 2.5 ml/min and was spray dried using a Buchi B290 Advanced Spray Dryer (Flawil, Switzerland). The dryer was equipped with a 0.7 mm diameter nozzle and was operated with an air outlet temperature of 100°C and the atomizing air gauge set to 50 from a 6 bar source. The aspirator was set to 100%.

2.2 Ultramicrotomy

Micro-particle powders without trehalose were embedded in epoxy resin modified after Kushida [39]. The resin mixture used was 9 g Quetol 651 (Ethylene glycol diglycidyl ether), 11.6 g NSA (Nonenyl Succinic Anhydride hardener), 5 g MNA (Methyl Nadic Anhydride) and 0.5 g BDMA (Benzydimethyamine) (Agar Scientific Ltd, UK).

To achieve uniform micro-particle dispersion the powder was suspended in 4% agar at 40°C. Droplets of agar solution were then gelled rapidly by pipetting the solution onto a glass microscope slide previously chilled to 4°C. Small pieces of microparticle containing agar were then transferred to vials containing cold 70% ethanol and subsequently dehydrated by multiple exchanges of the ethanol solution for progressively higher ethanol concentrations up to 100% ethanol. This was followed by 2 changes in dry 100% acetonitrile. They were then incubated in a 50% acetonitrile/50% resin mixture without catalyst and then just resin without catalyst. To ensure full infiltration with resin, five daily changes of the catalyst-free resin were made followed by five daily changes of resin with catalyst. Pieces of fully infiltrated agar were then placed in coffin moulds together with degassed resin. Air was excluded from these moulds by covering them with a thin Aclar sheet (Agar) and the resin was cured at 60°C for 24 h. They were sectioned with a 45° wedge angle diamond knife (Diatome, Switzerland) using a microtome (Reichert Jung, Ultracut E. Leica, Vienna) and floated out onto copper grids with minimum dwell time in the water bath. The use of a 35° or lower wedge angle diamond knife was not necessary as un-sintered HA is relatively soft.

2.3 TEM

Thin sections were imaged using an FEI CM100 operated at 100 KeV or an FEI Tecnai 20 operated at 200 keV. The Tecnai 20 was used to obtain selected area electron diffraction (SAED) patterns at a camera length of 890 mm. An oriented single crystal gold film (Agar) was used as a calibration standard for the estimation of lattice spacings from SAED patterns. Exposure of the region of interest to the electron beam was minimised by obtaining best focus, astigmatism and brightness on a region adjacent to region of interest before exposing the region of interest to the electron beam for <5 s to obtain an image.

2.4 FIB milling

Specimens were milled in a dual-beam ESEM FIB instrument Quanta 3D (FEI Co., Hillsboro, OR, USA). Electrons from a tungsten source were accelerated to 5 or 10 KeV for secondary electron imaging. A liquid gallium ion source operating at 30 KeV was used for milling and ion imaging. Samples were mounted within the ESEM FIB on an SEM stub that was customized into a miniature vice that gripped a TEM grid so that the plane of the grid surface was near perpendicular to the surface of the stub.

2.5 Milling individual microparticles

MPs (Fig. 1a, b) were deposited on holey carbon films on copper finder grids (Type H7, Agar) grids to make it easier to relocate sectioned MPs in the TEM once they had been ion beam milled. MPs were either lightly sprinkled over the surface of the film grid as a dry powder or alternatively collected onto the grid by gently passing the grid through a dilute MP suspension in the non aqueous carrier fluid, perflourodecalin, which was then allowed to evaporate. The latter alternative gave nearer to optimal grid coverage with only a few particles per grid square.

Grids were then sputter coated with gold to minimise charging and clamped in the customised holder. Bending the grid by 3–5° towards the ion beam source proved advantageous when sectioning individual particles as they were less likely to be obscured by grid bars, when the sample was tilted. Once inside the ESEM FIB a suitable grid square containing several candidate particles was identified. This grid square was then placed at the eucentric point of the instrument, where the tilt axis of the stage and the optical axes of the electron beam and ion beam are coincident. The microscope stage was then tilted by 52° away from the optical axis of the electron beam and toward the ion source. A low ion beam current (3–10 pA) was then used to image the MPs. As the gallium ion beam continually erodes the sample during imaging precautions were taken to limit unnecessary exposure of MPs to the ion beam prior to milling. Continuous scanning of the MP was avoided. Instead, individual frames of the entire field of view were grabbed to pin point the particle's position. Astigmatism was corrected and optimal focus obtained before deciding what area would be milled. The milling process was interrupted at regular intervals to verify that the position of the particle being milled had not shifted during milling. Such shifts were common events even though particles were sputtered with gold prior to milling and meant a new candidate particle had to be selected. Excessive beam currents (>100 pA) would destroy or eject particles from the surface of the support film. Complete sections for the TEM, could not be fabricated either by

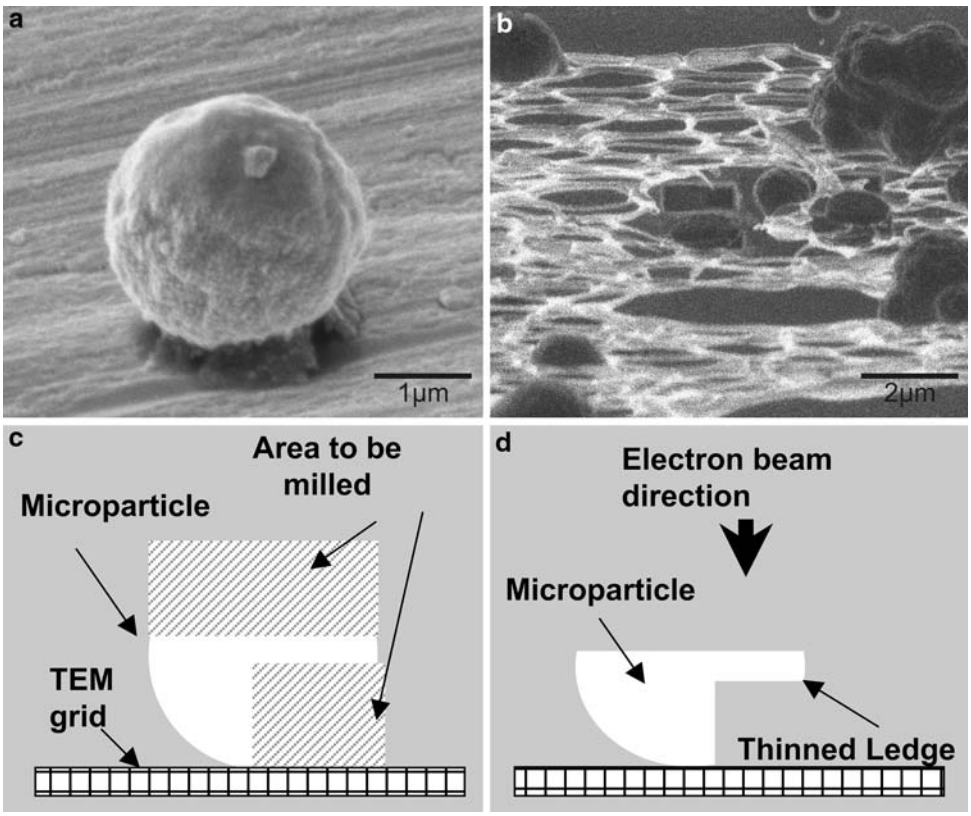

Fig. 1 (**a**) Secondary electron image of an individual MP (**b**) FIB image of MPs deposited onto a holey carbon film (**c**) schematic of MP illustrating portions to be FIB-Milled (**d**) schematic of milled MP with a ledge milled for viewing by TEM

milling away the top and bottom portions or opposing sides of a micro-particle. An overhang thin enough to reveal the hydroxyapatite nanoparticles by TEM, could be produced by milling away the upper hemisphere and about half the lower portion of the micro-particle, as illustrated schematically in Fig. 1c, d.

2.6 Encapsulation of microparticles for ion milling

MPs were encapsulated in a 1:1 ratio of particles to resin. Thick (~25 μm) slices of microparticle containing resin were then cut with a glass knife and mounted onto a parallel bar grid, sliced in half to allow access to the edge of the resin slice by the FIB (Fig. 2a).

Alternatively, MPs were mixed with silver dag bonded resin (RS Components Ltd, UK), which is a mixture of 2-Methoxy-1-methylethyl acetate n-butyl acetate and colloidal silver flakes.

Samples for milling were prepared by placing a drop of silver dag mixed with MPs on the leading edge of a half grid resting on a Teflon surface (Fig. 2b) or by compressing a drop of dag-MP mixture between two single hole gold, grids to form a sandwich that was subsequently cut along a cord to form an edge for milling (Fig. 2c).

MP sandwiches were clamped in the grid vice and the region for milling was placed at the eucentric point of the ESEM FIB. Prior to milling a 2 μm thick 2 μm wide platinum strap was deposited along the top of the region to be thinned, by decomposition of the metal-organic Pt-precursor (Trimethyl[(1,2,3,4,5-ETA.)-1 Methyl 2, 4-Cyclopentadien-1-YL] Platinum) by the Ga ion beam. This strap helps prevent unwanted ion beam erosion, or redeposition of ablated material and minimizes 'curtaining' artefacts that appear as uneven vertical striations on cross-sectioned faces [22]. Specimens were then progressively thinned into the appropriately named "H-section". Figure 3a shows the end on view of an ion beam image of the thinned sample. Figure 3b shows the secondary electron image of the plan view of this section. A relatively high ion beam current (20 nA) was used to coarsely mill away material either side of the region of interest leaving behind a ~3 μm thick lamella. A thinner lamella, ~1 μm thick was then milled with a reduced beam current of 300 pA or less. The axis of the sample was tilted away from the axis of the ion beam by 1–2° during the initial fine milling steps to compensate for the divergence of the FIB in order to produce a lamella of constant thickness. After fine milling the profile of individual micro-particles could be distinguished from the encapsulating matrix (Fig. 3d).

Coarse and fine milling steps were performed in the milling mode of the Quanta 3D where the ion beams rasters across an entire selected area. The lamella forming the final section was polished with a low beam current of 100 pA or less using the Quanta 3D's polishing mode. In this mode

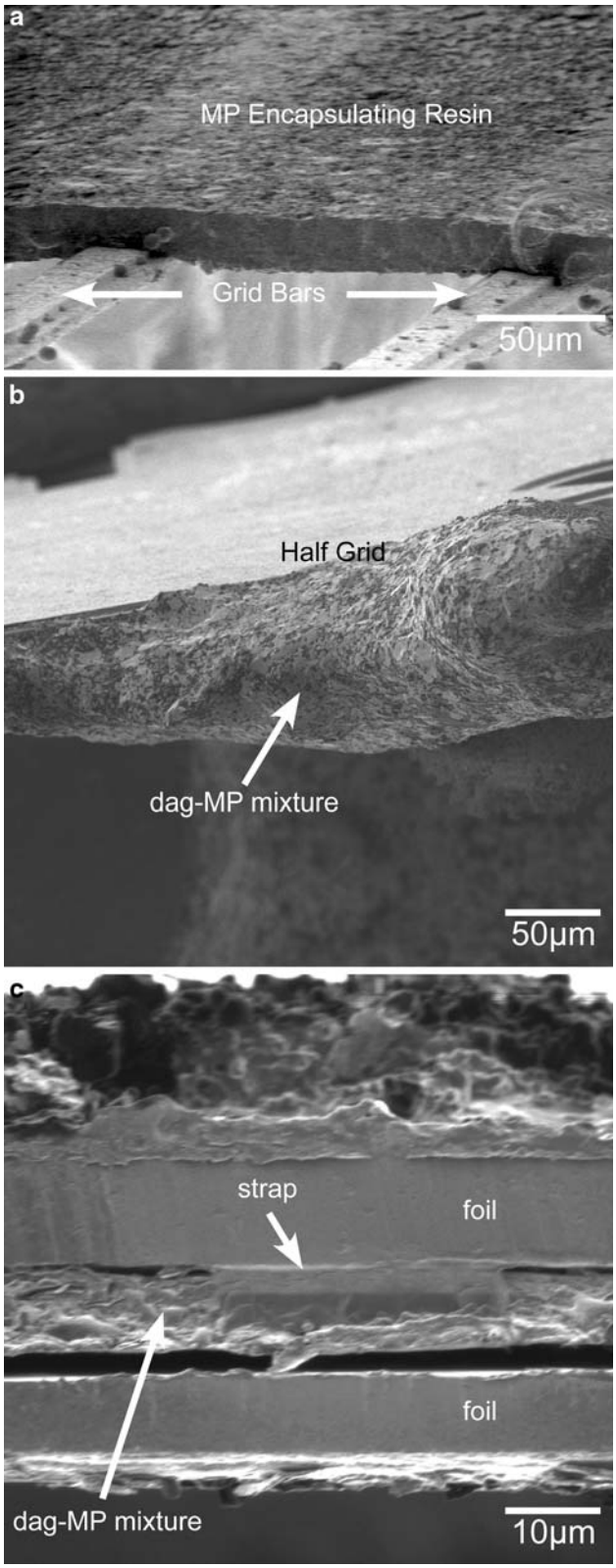

Fig. 2 (**a**) Slice of epoxy resin encapsulating MPs mounted on a parallel grid and bisected to allow access of the FIB to its edge. (**b**) Dag mixed with MP applied to the leading edge of a half grid. (**c**) Dag MP mixture sandwiched between two gold grids cut to form an edge for FIB milling

the ion beam was scanned repeatedly along single lines before scanning the next line. Images were obtained at regular intervals to monitor the progress of this final polishing step. Polishing was halted when obvious holes appeared in the thinned section. At this stage the profiles of the individual beads became less apparent from the surrounding matrix. The same precautions were taken to prevent unnecessary exposure of the thinned sections to the ion beam throughout their preparation. If during the fine or coarse milling stages the platinum strap was totally eroded it was replaced.

3 Results

3.1 Resin embedded microparticles

In the absence of a sugar matrix, resin can infiltrate between the NPs and into the MP's interior and once cured it mechanically stabilizes the MP for physical sectioning. Figure 4 shows TEM images of MPs spray dried from a sugarless suspension of HA NP's embedded in epoxy resin. These samples sectioned easily using a 45° wedge angle diamond knife. The MP profiles seen at low magnification varied from kidney-shaped to circular. Their 2D profiles were consistent with the 3D corpuscular morphology observed by SEM. At higher magnification (Fig. 4d) individual NPs were clearly discerned and were indistinguishable from NPs imaged by drying a dilute nanoparticle suspension onto a carbon film (Fig. 4e). Spaces in the order of 10 nm were also evident between NPs imaged at higher magnification. Relatively, few fractures or knife marks were observed in appropriately embedded material although, nanoparticle material was found to occasionally fall out from sections leaving characteristic voids Fig. 5.

3.2 MPs individually milled using FIB-SEM

FIB-milling revealed that individual MPs with or without added sugar were composed of uniformly distributed NPs and that they are solid rather than hollow. Figure 6 shows ledges milled into an individual microparticle, containing 50% trehalose and 50% NPs. Individual nanoparticles could be resolved, although FIB milling can produce terraces with different thicknesses. Ledges took between 3 and 5 min to mill, so a large number of microparticles could be sectioned with this method in a short period of time. However, at least 50% of the attempts to mill ledges were unsuccessful. Often the film underlying the microparticle was eroded by the ion-beam or the micro-particle moved during milling. Also when they were transferred to the TEM some ledges were too thick to be imaged.

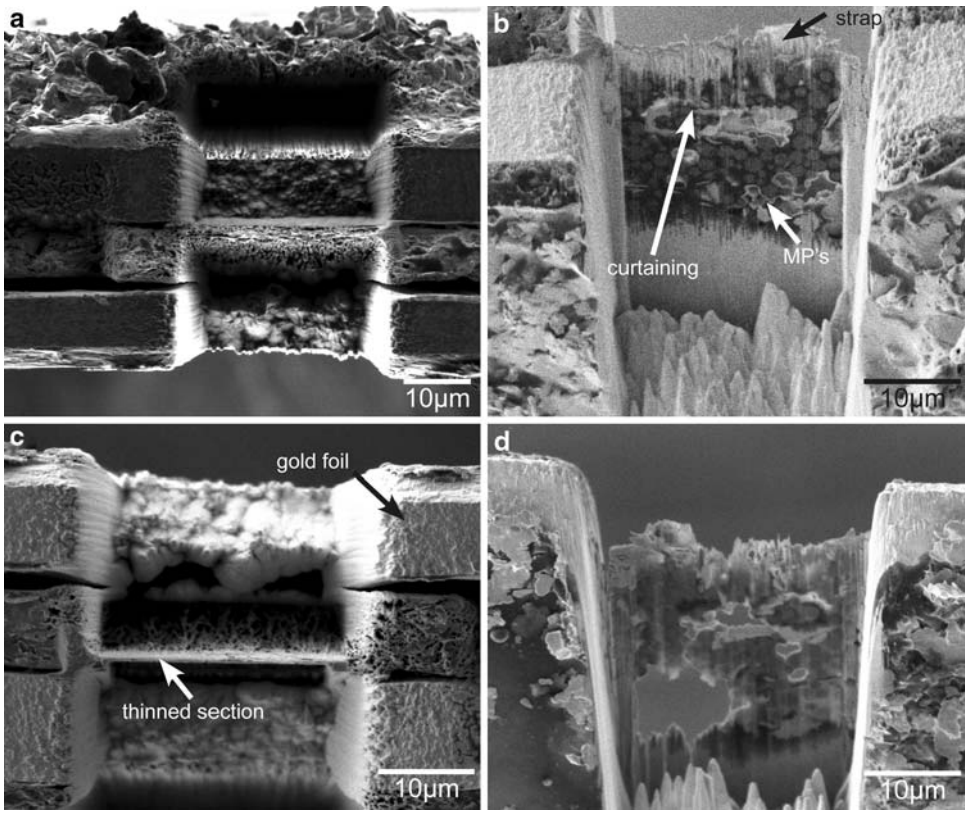

Fig. 3 Encapsulated material imaged during FIB-milling process: (**a**) FIB image of the cross section after coarse milling, (**b**) Secondary electron image of the side view after coarse milling, (**c**) end view, FIB image after fine milling, (**d**) side view, SE image after fine milling and polishing steps

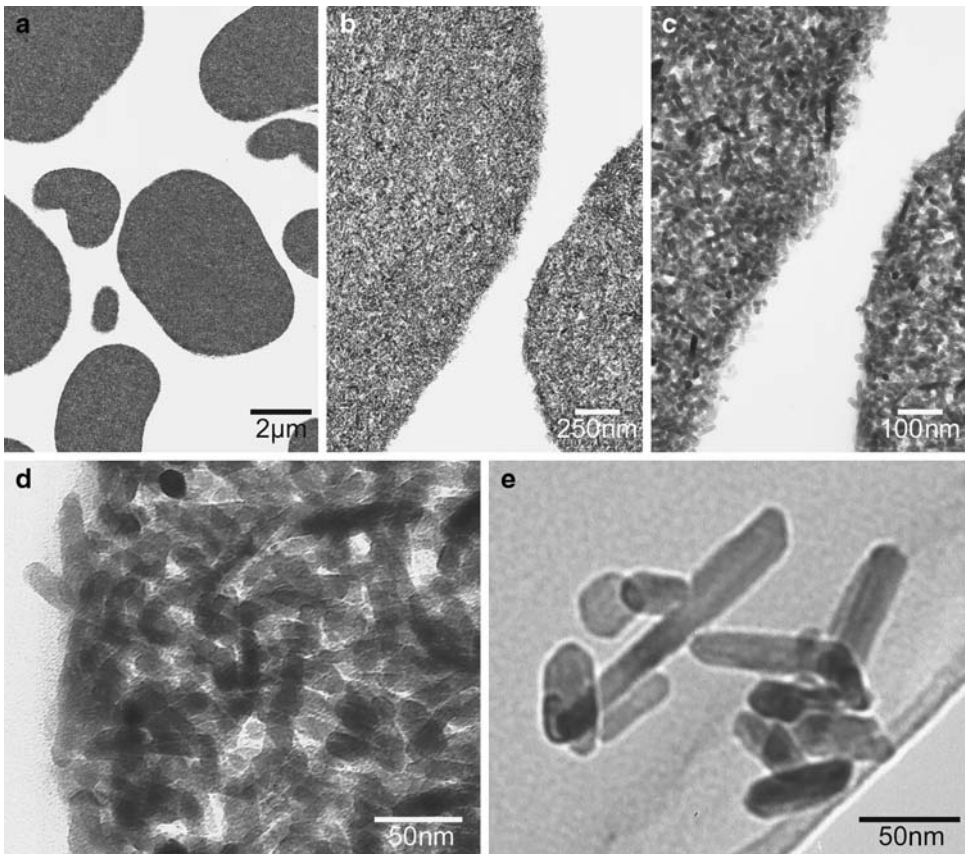

Fig. 4 TEM images of MPs spray dried without sugar sectioned using ultramicrotomy at progressively higher magnifications, (**a**) scale bar 2 μm, (**b**) scale bar 250 nm, (**c**) scale bar 100 nm, (**d**) scale bar 50 nm and, (**e**) individual NPs particles deposited onto holey carbon film (CM 100 operating at 100 keV)

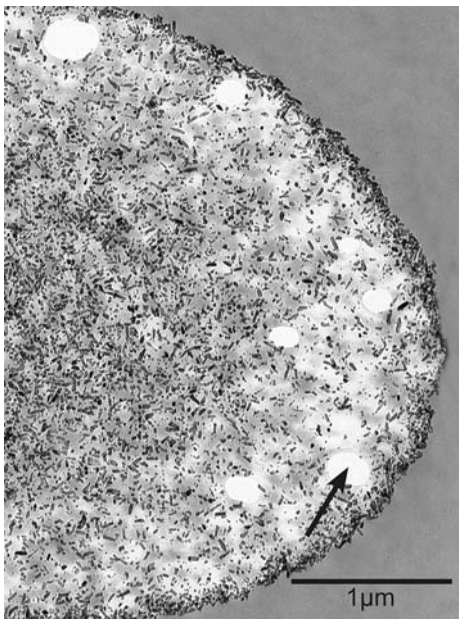

Fig. 5 TEM image of MPs spray dried without sugar sectioned by ultramicrotomy illustrating mechanical damage (scale bar 1 μm, CM 100 operating at 100 keV). Voids caused by nanoparticles falling out of the section are illustrated by arrows

3.3 Multiple MPs FIB-milled after encapsulation

After encapsulation in resin, or silver dag, large numbers of MPs could be milled together. This method was preferred, because it was quicker, the material was less prone to charging, and it worked well for MPs with both high and low sugar contents. Figure 7 shows TEM images of sections of microparticles containing decreasing amounts of Trehalose. NPs inside MPs containing 80% sugar (Fig. 7a) appeared more dispersed than in MPs with 50% sugar (Fig. 7b). With 80% sugar the space between NPs was in the same order of magnitude as the nanoparticle size ~50 nm. MPs with no sugar (Fig. 7c) did not appear any more tightly packed than those with 50% sugar.

3.4 Selected area electron diffraction patterns

Figure 8b, c, d shows SAED patterns obtained from aggregated NP's in a section of a sugar free microparticle that was FIB milled after encapsulation in resin (Fig. 8a). A series of rings consisting of discernible spots was obtained, consistent with the diffraction pattern from a polycrystalline sample. The brightest annulus of spots was of finite width corresponding to a lattice spacing between 2.4 and 2.8 Å although, most spots corresponded to a lattice spacing of 2.7 Å. Diffuse spots were also scattered around an annulus corresponding to a lattice spacing around 1.7 Å. When a smaller aperture was used and the beam was focussed on single NP's an array of spots was produced that was typical of the diffraction pattern obtained for a single crystal or a small number of crystallites.

4 Discussion

In the absence of a sugar matrix, embedding in epoxy resin followed by ultramicrotomy is the easiest method to produce thin sections of MP spray dried from HA NPs. MPs with a significant sugar-glass component cannot be infiltrated with epoxy resin. We have found FIB-milling is the only consistent method to produce thin sections of MPs containing sugar.

FIB-milling MPs scattered onto a TEM grid was initially chosen as the simplest way of revealing the internal arrangement of NPs with the MPs. It was time consuming and produced a very small number of sections suitable for TEM. The most common technique used for bulk materials is the "lift out" technique [40] where lamellae are milled into a specimen and placed on a grid by micromanipulation. Lift out procedures have been used on larger MPs, Volkert et al. [21] lifted lamellae 10 μm by 20 μm by 80 nm from large dumbbell shaped fluorapatite particles to avoid the fracture artefacts produced by ultramicrotomy.

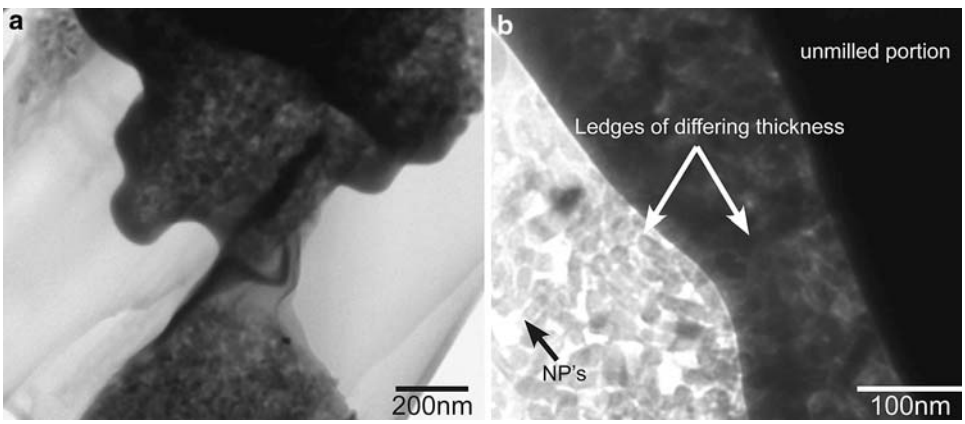

Fig. 6 TEM images of ledges FIB-milled MPs spray dried from 50% weight HA-NPs 50% trehalose, (**a**) scale bar 200 nm, (**b**) scale bar 100 nm (Technai 20 operating at 200 keV)

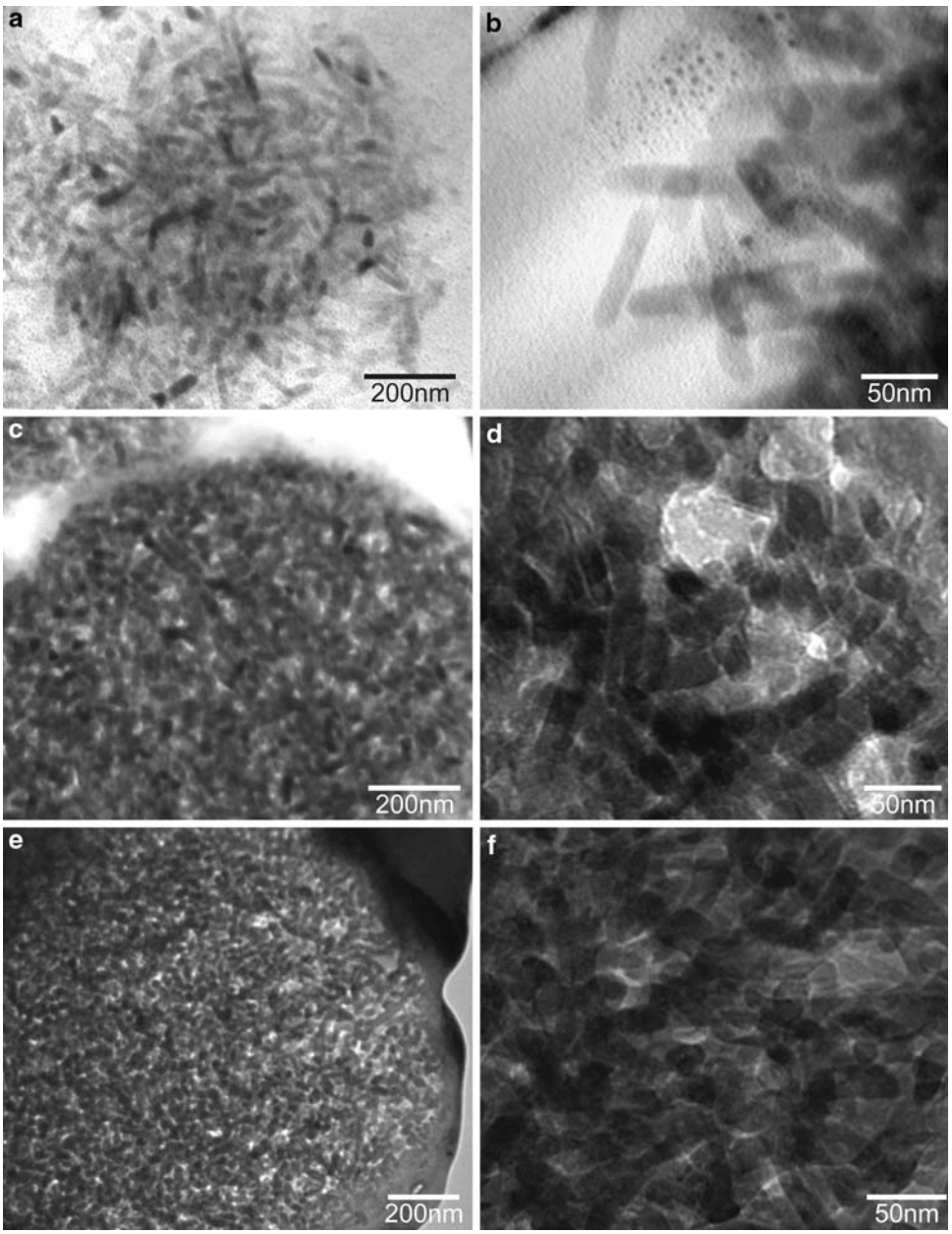

Fig. 7 TEM images of sections of MPs spray dried with various weight percentages of NPs sectioned by FIB-milling particles encapsulated in silver dag. (**a**) 20 wt% NPs scale bar 200 nm, (**b**) 20 wt% NPs scale bar 50 nm, (**c**) 50 wt% NPs scale bar 200 nm, (**d**) 50 wt% NPs scale bar 50 nm, (**e**) 100 wt% NPs scale bar 200 nm and, (**f**) 100 wt% NPs scale bar 50 nm (Technai 20 operating at 200 keV)

Lift out takes time and skill and is very technically demanding. Lifting micrometer sized sections from microparticles smaller than 10 micrometres is technically unfeasible. Methods that do not require manipulation of the thinned area are to be preferred where possible.

Volkert et al. [21] milled ledges into smaller particles below <20 μm in diameter on half grids and transferred them in situ on the grids to the TEM as an alternative to lifting and mounting thin lamellae. This method proved possible for the smaller particles we studied but was limited by practical considerations. It was only possible to mill ledges into MPs rather than to prepare complete sections through MPs so only partial information about a particle's internal arrangement was provided by this method. The ledges produced varied in thickness and until grids were viewed by TEM it was hard to establish if milled ledges were thin enough to distinguish their internal structure. Ledges were milled into several microparticles at a time and it took over an hour to successfully produce a particle with a suitably thin ledge.

During milling the optical axis of the FIB is parallel to the surface of interest to minimise ion penetration into the thin specimen. Milling this way limits any preferential etching but causes an artefact known as "curtaining" [9]. This artefact manifests itself on the surface being milled as terraces of varying thickness that run parallel to the incident ion beam [41] and are a memory of the interaction of the rastering ion beam with the material being ablated. This

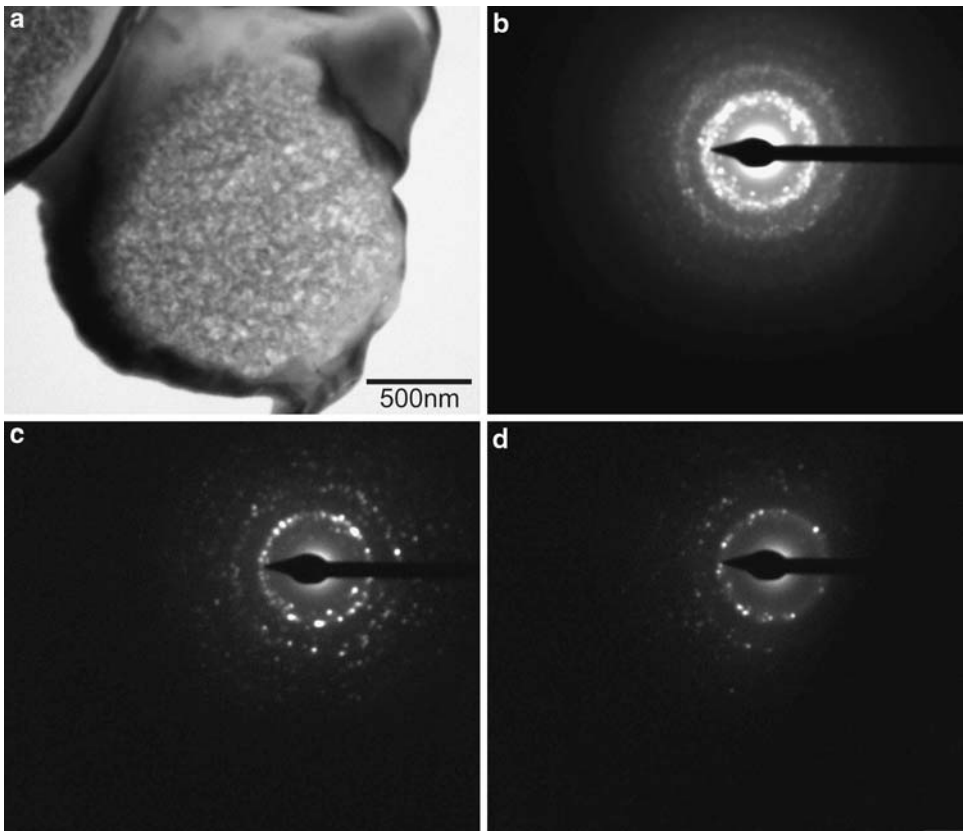

Fig. 8 (**a**) Brightfield TEM image of sections of sugarless MP FIB-milled following encapsulation in silver dag obtained and the selected area electron diffraction patterns obtained with progressively narrow apertures (**b–d**) from this section

is unavoidable in most FIB-milling procedures and is especially prevalent when milling heterogeneous samples containing materials with differing sputter yields [42]. The degree of curtaining depends on the heterogeneity of a material, its resistance to ion beam ablation and the initial rugosity of its surface [43]. Depositing a strap of conducting metal smoothens the surface and reduces curtaining [43]. The terraces observed after milling individual MPs (Fig. 6) are a manifestation of curtaining and may be expected since the hydroxyapatite is likely to have more resistance to ion ablation than the sugar matrix.

Encapsulating MPs in resin or silver dag for FIB milling had several advantages over milling individual MP's. They were completely cross-sectioned, instead of being partially sectioned and many particles could be sectioned at once. This preparation also allowed a platinum strap to be deposited along the edge to be milled to limit curtaining. Fine polishing steps at progressively lower current should be performed to remove any curtaining, evident after coarse milling (Fig. 3c) and any sputtered material that was re-deposited during coarse milling. Grids with "H" shaped sections cut into encapsulated material could be manipulated carefully with forceps without destroying the thinned region and samples could be returned to the ESEM/FIB for further polishing if the thinned region was found to be too thick.

Epoxy resin is an obvious choice of encapsulating medium since it is very stable in the TEM beam. Mixing resin with microparticles in an approximately 1:1 ratio was sufficient to achieve a high MP concentration and adequate section stability during milling. Cairney and Munroe [44] found it necessary to concentrate microsized particles by centrifuging them in the resin before curing when FIB-milling FeAl and WC powders encapsulated in Spurr's resin. In this case sections must be made parallel to the sedimentation axis if the whole population of particles is to be sampled.

Epoxy resin was susceptible to charging in both the ion and electron beams. Coating with an adequate layer of gold (50 nm) before milling reduced charge accumulation during the initial stages of milling. Charge accumulation often caused the region being milled to physically move. It also caused image drift and degraded the contrast of images captured to monitor milling during the final polishing steps. If the region being thinned is regularly scrutinised and repositioned when necessary, it is perfectly possible to thin resin sections for TEM inside the FIB. Such charging effects can be suppressed inside the ESEM FIB using charge compensation where charging by the ion-beam is balanced by a defocused, low energy, electron beam [45].

To reduce charging the use of a conductive encapsulant is to be recommended. Encapsulating microparticles, in

silver dag to prevent the specimen shifting also improved the quality of the images taken to monitor the milling progress. This method of encapsulation was also much quicker than resin embedding. Resin blocks are cured by heating to 60°C for 18 h whilst silver dag hardens in minutes. The silver dag was fashioned into a suitable shape for FIB-milling before it dried, as it was too soft to be shaped mechanically. Sandwiching a silver dag-powder layer between two disk shaped foils was preferred, because it resulted in a thinner assembly (<30 μm) that required less coarse milling. The cut edges of the gold foils also acted as a guide for milling and providing a good conducting pathway that reducing charging. This preparation was also found to be robust when it was transferred from the ESEM FIB to the TEM after milling.

Despite depositing a protective platinum strip, milling obliquely to the surface of the section and using fine polishing steps, the interaction with the ion beam extends into both sides of the section. This can damage the thinned sample by implanting ions, creating point defects and, dislocations and, in extreme cases causing, phase changes [46]. Electron beam induced damage in HA is a radiolytic damage process involving the loss of phosphorous and oxygen, amorphization and ultimately crystallization to form CaO. If a 200 keV electron beam is used these effects will occurr at fluences greater than 10^8 electrons nm^{-2} [47]. To avoid these effects exposure of the sample to the electron beam was kept to a minimum when obtaining images by TEM. The available literature on ion beam interactions with apatite mostly deals with high energy, ions generated from fission. Such high energy ions can completely convert crystalline apatite into amorphous material [48]. Amorphous damage layers raise the background noise intensity in TEM images and reduce image contrast [49]. Little information is available about how glancing angle gallium ion beams in the 10–30 keV range interact with apatite during milling and most studies of ion beam interactions during FIB milled have concentrated on semiconductor materials, in particular silicon. Monte Carlo modelling of the interaction of the 30 keV gallium ion beam with Si, suggests that the amorphous zone extends ~20 nm into the Si, in agreement with experimental observations [50]. Alexandre et al. [51] suggest that using a low current (55 pA) and low voltage (10 kV) reduces the depth of the amorphous zone to 7 nm in Si. For GaAs the layer of complete amorphization caused by a (30 KeV, 100 pA) beam extends 20 nm into a sample, although the "inactive" thickness extends more than 200 nm [52]. This indicates that the ion beam changes to the sample may penetrate deeper than 20 nm. Unfortunately no useful simulations of ion beam sample interaction exist for HA. According to Monte Carlo model trajectories of ions striking a sidewall at a glancing angle extend 20 nm into $CaCO_3$ and over 50 nm into organic matter with a generic formula CH_2O [15]. Wuchel et al. recently found that a 5 KeV Ga ion beam incident at an angle of 45° onto a trehalose film results in a maximal ion concentration at a depth of 30 nm [53]. By inference ion beam damage of hydroxyapatite crystallites and sugar could, therefore extend through, the entire thickness of a TEM section. SAED patterns for milled MP indicate they are crystalline after milling and not amorphous. However, it is difficult to distinguish between the reflections corresponding to CaO and HA due to their proximity. The 3rd brightest [111] reflections for CaO corresponds to a lattice spacing of 2.78 Å according to reference pattern (ICDD 00-037-1497) which essentially over laps with the [211], [112] and [300] reflections corresponding to lattice spacings of 2.81, 2.77, 2.72 Å that are the brightest for HA according to reference pattern (ICDD 01-074-0565). There were few spots observed that corresponded to the brightest [200] reflections for CaO corresponding to a lattice spacing of 2.41 Å. Indicating relatively little conversion from HA though amorphous material to crystalline CaO had occurred. Such changes would also be accompanied by gross changes in NP morphology, similar to those caused by long term exposure to the electron beam. A quantitative study, similar to that undertaken by Eddisford et al. [47] on HA exposure to the electron beam during TEM determining the Ca/P ratio by EDX or EELS of HA as function of beam current, energy and total beam exposure, that studies ion beam damage to HA is now warranted . However, in this study of the nanoporosity of MP from NPs such changes are irrelevant. Ion beam interactions with amorphous materials can cause recrystallisation. In a proof of concept study using the Cryo-FIB to section frozen hydrated cells Marko et al. [54] found that a 30 KeV, 10 pA beam was insufficient to devitrify ice. A similar study should perhaps be performed for sugars to confirm that the ion beam interaction during milling does not cause localised heating and devitrification of the sugar glass. These all indicate that if probe currents are controlled during polishing, artefacts can be minimised.

TEM images showed more space between NPs in MP containing 80% sugar than in those containing 50% or no sugar. This has implications for slow-release and the toxicological behaviour of the vaccine system. Contact between nanoparticles during spray drying causes them to fuse giving the MPs structural integrity. MPs spray dried in the absence of sugar and soaked in Simulated Body Fluid at pH 7.4 show little if any structural disintegration after 3 months. MPs containing 80% sugar disintegrate entirely upon contact with water into free NPs whilst those with 50% sugar only partially disintegrate. After injection in vivo, MPs that contain mostly sugar will immediately release a large number of antigen bearing, potentially toxic NPs at the injection site that can enter cells, by various

mechanisms. Those without sugar will remain intact until scavenged and engulfed by macrophages where they may slowly dissolve causing NPs to be shed over a much longer time course.

Determining the precise thickness of ultrathin TEM sections is non trivial [55, 56] and as NPs have one dimension thinner that typical thin sections (50–70 nm) small variations in thickness between sections will cause artefacts. Estimating the volume fraction of the MP occupied by the NPs and that occupied by the sugar or free space between NP will require precise control of section thickness and has not been included in this study. An alternative method to examine inter-particle space is electron tomography. FEG-SEM can resolve individual HA nanoparticles and as the latest generation of FIB-SEMs, are capable of a volumetric resolution of 17 nm^3 [57], FIB serial sectioning and image capture could be used to generate 3D reconstructions of MP ultrastructure. Electron backscattered imaging at low accelerating voltages can be used to distinguish the NPs from the sugar glass and enhance the precision of the subsequent reconstruction. Milling slices with the intense central portion of the FIB beam limits the minimum slice width to about 20 nm comparable to the width of individual HA NPs. Using the tail of the FIB beam [58] it is possible to ablate 2 nm slices.

5 Conclusion

Sections generated by FIB-milling showed a clear difference in nanoporosity between microparticles containing no trehalose, 50% trehalose or 80% trehalose. Sections could be readily prepared from resin embedded HA microparticles using a 45° wedge angle diamond knife with minimal sectioning artefacts. It was impossible to infiltrate microparticles containing trehalose with epoxy resin. FIB-Milling is the only method currently available to generate sections of HA-sugar glass composites. FIB-milling eliminates the need for much of the extended, multi-stage chemical fixation and embedding required to section MPs by ultramicrotomy. It also reduces mechanical artefacts.

Acknowledgments This work was funded by a DTI grant (CHBS/004/00063C) held jointly by J. N. Skepper at the University of Cambridge and Cambridge Biostability Ltd. The Dual Beam FIB/ESEM was purchased with funds from the BBSRC.

References

1. R.K. Nalla, A.E. Porter, C. Daraio, A.M. Minor, V. Radmilovic, E.A. Stach et al., Micron **36**, 672 (2005). doi:10.1016/j.micron.2005.05.011
2. A.E. Porter, R.K. Nalla, A. Minor, J.R. Jinschek, C. Kisielowski, V. Radmilovic et al., Biomaterials **26**, 7650 (2005). doi:10.1016/j.biomaterials.2005.05.059
3. A.E. Porter, N. Patel, J.N. Skepper, S.M. Best, W. Bonfield, Biomaterials **25**, 3303 (2004). doi:10.1016/j.biomaterials.2003.10.006
4. C. Quintana, Micron **28**, 217 (1997). doi:10.1016/S0968-4328(97)00023-1
5. G. Mcmahon, T. Malis, Microsc. Res. Tech. **31**, 267 (1995). doi:10.1002/jemt.1070310403
6. P. Swab, Microsc. Res. Tech. **31**, 308 (1995). doi:10.1002/jemt.1070310408
7. L.A. Giannuzzi, F.A. Stevie, Micron **30**, 197 (1999). doi:10.1016/S0968-4328(99)00005-0
8. J.A.W. Heymann, M. Hayles, I. Gestmann, L.A. Giannuzzi, B. Lich, S. Subramaniam, J. Struct. Biol. **155**, 63 (2006). doi:10.1016/j.jsb.2006.03.006
9. R.M. Langford, Microsc. Res. Tech. **69**, 538 (2006). doi:10.1002/jemt.20324
10. M.W. Phaneuf, Micron **30**, 277 (1999). doi:10.1016/S0968-4328(99)00012-8
11. M.D. Uchic, L. Holzer, B.J. Inkson, E.L. Principe, P. Munroe, MRS Bull. **32**, 408 (2007)
12. D. Drobne, M. Milani, V. Leser, F. Tatti, Microsc. Res. Tech. **70**, 895 (2007). doi:10.1002/jemt.20494
13. H. Engqvist, G.A. Botton, M. Couillard, S. Mohammadi, J. Malmstrom, L. Emanuelsson et al., J. Biomed. Mater. Res. A **78A**, 20 (2006). doi:10.1002/jbm.a.30696
14. H. Engqvist, F. Svahn, T. Jarmar, R. Detsch, H. Mayr, P. Thomsen et al., J. Mater. Sci. Mater. Med. **19**, 467 (2008). doi:10.1007/s10856-006-0042-9
15. M. Obst, P. Gasser, D. Mavrocordatos, M. Dittrich, Am. Mineral. **90**, 1270 (2005). doi:10.2138/am.2005.1743
16. A. Heeren, C. Burkhardt, H. Wolburg, W. Henschel, W. Nisch, D.P. Kern, Microelectron. Eng. **83**, 1602 (2006). doi:10.1016/j.mee.2006.01.114
17. S. Kumar, W.A. Curtin, Mater. Today **10**, 34 (2007). doi:10.1016/S1369-7021(07)70207-9
18. L.F. Dobrzhinetskaya, R. Wirth, H.W. Green, Proc. Natl. Acad. Sci. USA **104**, 9128 (2007). doi:10.1073/pnas.0609161104
19. Y. Hayashi, T. Yaguchi, K. Ito, T. Kamino, Scanning **20**, 234 (1998)
20. K. Hoshi, S. Ejiri, W. Probst, V. Seybold, T. Kamino, T. Yaguchi et al., J. Microsc. **201**, 44 (2001). doi:10.1046/j.1365-2818.2001.00784.x
21. C.A. Volkert, S. Busch, B. Heiland, G. Dehm, J. Microsc. **214**, 208 (2004). doi:10.1111/j.0022-2720.2004.01352.x
22. M.F. Hayles, D.J. Stokes, D. Phifer, K.C. Findlay, J. Microsc. **226**, 263 (2007). doi:10.1111/j.1365-2818.2007.01775.x
23. M. Marko, C. Hsieh, R. Schalek, J. Frank, C. Mannella, Nat. Methods **4**, 215 (2007). doi:10.1038/nmeth1014
24. J.E.M. Mcgeoch, J. Microsc. **227**, 172 (2007). doi:10.1111/j.1365-2818.2007.01798.x
25. M.J. Gorbunoff, Methods Enzymol. **117**, 370 (1985). doi:10.1016/S0076-6879(85)17022-9
26. M.J. Gorbunoff, Methods Enzymol. **182**, 329 (1990). doi:10.1016/0076-6879(90)82028-Z
27. T. Matsumoto, M. Okazaki, M. Inoue, S. Yamaguchi, T. Kusunose, T. Toyonaga et al., Biomaterials **25**, 3807 (2004). doi:10.1016/j.biomaterials.2003.10.081
28. B.G. Santoni, G.E. Pluhar, T. Motta, D.L. Wheeler, Biomed. Mater. Eng. **17**, 277 (2007)
29. M.P. Ferraz, A.Y. Mateus, J.C. Sousa, F.J. Monteiro, J. Biomed. Mater. Res. A **81A**, 994 (2007). doi:10.1002/jbm.a.31151
30. A. Slosarczyk, J. Szymura-Oleksiak, B. Mycek, Biomaterials **21**, 1215 (2000). doi:10.1016/S0142-9612(99)00269-0
31. A. Uchida, Y. Shinto, N. Araki, K. Ono, J. Ortho. Res. **10**, 440 (1992)
32. A. Barroug, M.J. Glimcher, J. Ortho. Res. **20**, 274 (2002)

33. M. Imamura, T. Seki, K. Kunieda, S. Nakatani, K. Inoue, T. Nakano et al., Oncol. Rep. **2**, 33 (1995)
34. C.C. Ribeiro, C.C. Barrias, M.A. Barbosa, Biomaterials **25**, 4363 (2004). doi:10.1016/j.biomaterials.2003.11.028
35. M.P. Ginebra, T. Traykova, J.A. Planell, J. Control. Release **113**, 102 (2006). doi:10.1016/j.jconrel.2006.04.007
36. P. Luo, T.G. Nieh, Biomaterials **17**, 1959 (1996). doi:10.1016/0142-9612(96)00019-1
37. K.A. Hing, Int. J. Appl. Ceram. Technol. **2**, 184 (2005). doi:10.1111/j.1744-7402.2005.02020.x
38. P.N. Kumta, C. Sfeir, D.H. Lee, D. Olton, D. Choi, Acta Biomater. **1**, 65 (2005). doi:10.1016/j.actbio.2004.09.008
39. H. Kushida, J. Electron. Microsc. Tokyo **23**, 197 (1974)
40. L.A. Giannuzzi, J.L. Drown, S.R. Brown, R.B. Irwin, F. Stevie, Microsc. Res. Tech. **41**, 285 (1998). 10.1002/(SICI)1097-0029(19980515)41:4<285::AID-JEMT1>3.0.CO;2-Q
41. J.M. Cairney, P.R. Munroe, Micron **34**, 97 (2003). doi:10.1016/S0968-4328(03)00007-6
42. P. Gasser, U.E. Klotz, F.A. Khalid, O. Beffort, Microsc. Microanal. **10**, 311 (2004). doi:10.1017/S1431927604040413
43. T. Ishitani, T. Yaguchi, Microsc. Res. Tech. **35**, 320 (1996). doi:10.1002/(SICI)1097-0029(19961101)35:4 ≤ 320::AID-JEMT3 ≥ 3.0.CO;2-Q
44. J.M. Cairney, P.R. Munroe, Mater. Charact. **46**, 297 (2001). doi:10.1016/S1044-5803(00)00107-8
45. D.J. Stokes, T. Vystavel, F. Morrissey, J. Phys. D Appl. Phys. **40**, 874 (2007). doi:10.1088/0022-3727/40/3/028
46. D.J. Barber, Ultramicroscopy **52**, 101 (1993). doi:10.1016/0304-3991(93)90025-S
47. P. Eddisford, A. Brown, R. Brydson, J. Phys.: Conf. Ser. **126**, 012008 (2008)
48. A. Meldrum, L.M. Wang, R.C. Ewing, Am. Mineral. **82**, 858 (1997)
49. S. Rubanov, P.R. Munroe, Micron **35**, 549 (2004). doi:10.1016/j.micron.2004.03.004
50. W. Boxleitner, G. Hobler, V. Kluppel, H. Cerva, Nucl. Instrum. Methods Phys. Res. Sect. B-Beam Interact. Mater. Atoms **175**, 102 (2001)
51. L. Alexandre, K. Rousseau, C. Alfonso, W. Saikaly, L. Fares, C. Grosjean et al., Micron **39**, 294 (2008). doi:10.1016/j.micron.2007.01.005
52. D. Cooper, R. Truche, J.-L. Rouviere, Ultramicros **108**, 488 (2008). doi:10.1016/j.ultramic.2007.08.006
53. A. Wucher, J. Cheng, N. Winograd, Anal. Chem. **79**, 5529 (2007). doi:10.1021/ac070692a
54. M. Marko, C. Hsieh, W. Moberlychan, C.A. Mannella, J. Frank, J. Microsc. **222**, 42 (2006). doi:10.1111/j.1365-2818.2006.01567.x
55. D.M.G. Degroot, J. Microsc. **151**, 23 (1988)
56. M.A. Aronova, Y.C. Kim, G. Zhang, R.D. Leapman, Ultramicros **107**, 232 (2007). doi:10.1016/j.ultramic.2006.07.009
57. FEI Company (2000) Technical Note No. PN 25564-C
58. T.S. Yeoh, N.A. Ives, N. Presser, G.W. Stupian, M.S. Leung, J.L. Mccollum et al., J. Vac. Sci. Technol. B **25**, 922 (2007). doi:10.1116/1.2740288